filter element. Thus, when the filter element is installed in the groove, the part of its wall that enters the groove with an interference fit is plastically deformed through plastic deformation of the walls of the interpore channels, which ensures a reliable seal between the filter element and the guide device. At the bottom end, the filter element is pressed by spring 6 through a baffle plate 5, which prevents possible loss of tightness of the filter element under vibration and dynamic loads on the filter. The baffle plate is mounted with a diametral clearance of 2–3 mm relative to bowl 2. The volume between the baffle plate and the bottom of the bowl forms a settling chamber. This design of the settling chamber prevents the sediment from entering the working filtration zone when the entire assembly is subjected to considerable oscillations.

For diesel engines with a power of up to 100 hp (≈ 74 kW), the overall dimensions of the assembled filter are as follows: outer diameter of the bowl, 45 mm; height, 110 mm.

Despite the substantial cost of PTFE as a raw material for filter element production, the cost of fuel cleaning with one such filter element over its full service life (taking into account repeated regeneration) is 2–3 times lower than with several filters having paper filter elements.

The authors acknowledge the use of Claude AI (Anthropic) for English translation and language editing of the manuscript.

## References

1. Kaleem M. A., Alam M. Z., Rehman S. U. An investigation on the malfunctioning of fuel injectors due to contamination of water in diesel fuel. Int. Trans. J. Eng., Manage., Appl. Sci. Technol. 2019. Vol. 10, no. 14. P. 1–6. Paper ID: 10A14M. ISSN 2228-9860. DOI: 10.14456/ITJEMAST.2019.191.
2. Krasiński A., Sołtan Ł., Kozyrski J. The effect of solids on interfacial rheology and the performance of coalescence filters. Chem. Process Eng. 2021. Vol. 42, no. 4. P. 337–348. DOI: 10.24425/cpe.2021.138934.
3. Kalyuzhny A. B., Karpova T. L., Kalyuzhny B. G., Platkov V. Ya. Structure and functional properties of high-porosity material based on Fluoroplast-4. Funct. Mater. 1999. Vol. 6, no. 2. P. 25–30.
4. Kaliuzhnyi O. B., Platkov V. Ya. The structure and properties of porous poly(tetrafluoroethylene). J. Polym. Res. 2022. Vol. 29, no. 1. Article 32. DOI: 10.1007/s10965-022-02887-w.
5. Калюжный А. Б., Платков В. Я., Калюжный Б. Г. Формирование давлением структуры и свойств пористых материалов на основе фторопласта-4 [Pressure formation of the structure and properties of porous materials based on fluoroplast-4]. Вісн. ХНТУСГ. 2017. Вип. 183. С. 39–44. [In Russian].

UDC 678.742.2:544.272:631.24

# MULTIFRACTAL MODEL OF GAS DIFFUSION IN POLYETHYLENE FOR PREDICTING THE BARRIER PROPERTIES OF POLYMER MATERIALS IN THE AGRO-INDUSTRIAL COMPLEX

***Lymar O.O.**, PhD (Physics and Mathematics), Associate Professor*
***Marchenko D.D.**, PhD (Engineering), Associate Professor*
*Mykolaiv National Agrarian University, Mykolaiv, Ukraine*

**Problem statement.** Polyethylene (PE) is the main polymer material of the agro-industrial complex (AIC): it is used to manufacture silage and haylage films, greenhouse and mulch films, grain storage bags, drip irrigation pipes, tanks for fuel and agrochemicals, and seals for agricultural machinery units [1]. The performance of such products is determined primarily by their gas permeability. In particular, oxygen penetration through the covering film is the main cause of aerobic spoilage of the top silage layer: according to a meta-analysis [2], dry matter losses in the top layer under standard PE film amount to 19.5 % versus 11.4 % under an oxygen barrier film, while the oxygen transmission rate of a standard 125 μm film is more than 100 times higher than that of a barrier film [3]. At the same time, the degradation of polymer and composite

materials under AIC operating conditions depends substantially on their structure [4, 5]. Therefore, an urgent scientific and practical task is to establish a quantitative relationship between the nanostructure of PE and the gas diffusion coefficient.

**Analysis of recent research and publications.** Studies of polymer nanostructure by scanning tunnelling microscopy and small-angle neutron and X-ray scattering indicate a hierarchy of supramolecular organization. Depending on the degree of ordering, PE macromolecules exist in amorphous and crystalline phases whose dimensions reach several tens of nanometres; in the amorphous phase, macromolecules form fractal clusters with a radius of about 3.5 nm. Gas permeability of polymers depends substantially on the degree of crystallinity, thermomechanical history, and the size and nature of penetrant molecules [6]. Systematic experimental data on the permeability, diffusion and solubility of gases in PE are given in [7, 8]. It has been established that PE melt has a monofractal structure, whereas the solid polymer is multifractal: for the melt, the diffusion coefficient $D$ is practically independent of the size of gas molecules, while for solid PE it decreases as their diameter $d_M$ increases. This is explained by the size distribution of free-volume microvoids. Substances in the amorphous state are metastable; therefore, by changing external factors, in particular heat treatment modes, their physical and mechanical properties can be controlled [9]. Thus, the problem of quantitative description of gas transport in PE taking into account the multifractal structure remains relevant.

**The aim of the study** is to substantiate a multifractal model of gas diffusion in solid polyethylene and to assess the possibility of its use for predicting the barrier properties of AIC polymer materials.

**Research results.** In amorphous-crystalline polymers, not the entire amorphous phase participates in diffusion, but only the part containing fluctuation free-volume microvoids with a diameter $d_h \geq d_M$. The fraction of the amorphous phase accessible for diffusion is determined as follows:

$$\alpha_{am}^{acc} = \alpha_{am} \cdot P_h(d_M) \quad (1)$$

where $\alpha_{am}$ is the volume fraction of the amorphous phase; $P_h(d_M)$ is the probability of finding a microvoid with a diameter $d_h \geq d_M$ in the polymer. Within the multifractal model,

$$P_h(d_M) = \left(\frac{d_M}{c}\right)^{-d_f} \quad (2)$$

where $c$ is a constant equal to 0.1 nm; $d_f$ is the fractal dimension of the polymer structure; for amorphous-crystalline PE, $d_f = 2.75$.

The decrease in the diffusion coefficient of solid PE compared with the melt is determined by the probability $P_h(d_M)$:

$$D = D_{am} \cdot P_h(d_M) \quad (3)$$

where $D_{am}$ is the diffusion coefficient of fully amorphous PE (melt), $cm^2/s$.

Table 1 lists the values of $d_M$ for eight gases, the values of $P_h$ and $D_{am}$, as well as the theoretical $D^{theor}$ values calculated by (2), (3) and the experimental $D^{exp}$ diffusion coefficients for PE. The results are compared in Fig. 1.

For $H_2$, CO, $CH_4$, $C_2H_6$ and Ar, the discrepancy between $D^{theor}$ and $D^{exp}$ does not exceed 25 %, and the correlation coefficient between the logarithms of these values for all gases is 0.94. For large atoms of noble gases (Kr, Xe, Rn), the model overestimates the diffusion coefficient, which requires refinement of the fractal dimension $d_f$ for penetrants with $d_M > 0.32$ nm. All this does not contradict the physical meaning: as $d_M$ increases, the fraction of accessible free volume decreases according to a power law (Fig. 1a).

For AIC products, the gas flux density through a film of thickness $l$ is of practical importance:

$$J = \frac{D \cdot S \cdot \Delta p}{l} = \frac{P \cdot \Delta p}{l} \quad (4)$$

where $S$ is the gas solubility coefficient, $cm^3/(cm^3 \cdot Pa)$; $\Delta p$ is the partial pressure difference, Pa; $P=D \cdot S$ is the permeability coefficient.

Table 1 – Calculated and experimental characteristics of gas diffusion in polyethylene

| Gas | $d_M$, nm | $D_{am} \times 10^7$, $cm^2/s$ | $P_h$ | $D^{theor} \times 10^7$, $cm^2/s$ | $D^{exp} \times 10^7$, $cm^2/s$ |
|---|---|---|---|---|---|
| $H_2$ | 0.22 | 309 | 0.114 | 35 | 35 |
| Ar | 0.30 | 96 | 0.049 | 4.7 | 3.9 |
| Kr | 0.32 | 74 | 0.041 | 3.0 | 1.8 |
| CO | 0.32 | 72 | 0.041 | 2.9 | 3.1 |
| $CH_4$ | 0.33 | 66 | 0.038 | 2.5 | 2.0 |
| Xe | 0.36 | 50 | 0.030 | 1.5 | 0.6 |
| Rn | 0.37 | 42 | 0.027 | 1.1 | 0.4 |
| $C_2H_6$ | 0.41 | 29 | 0.021 | 0.6 | 0.8 |

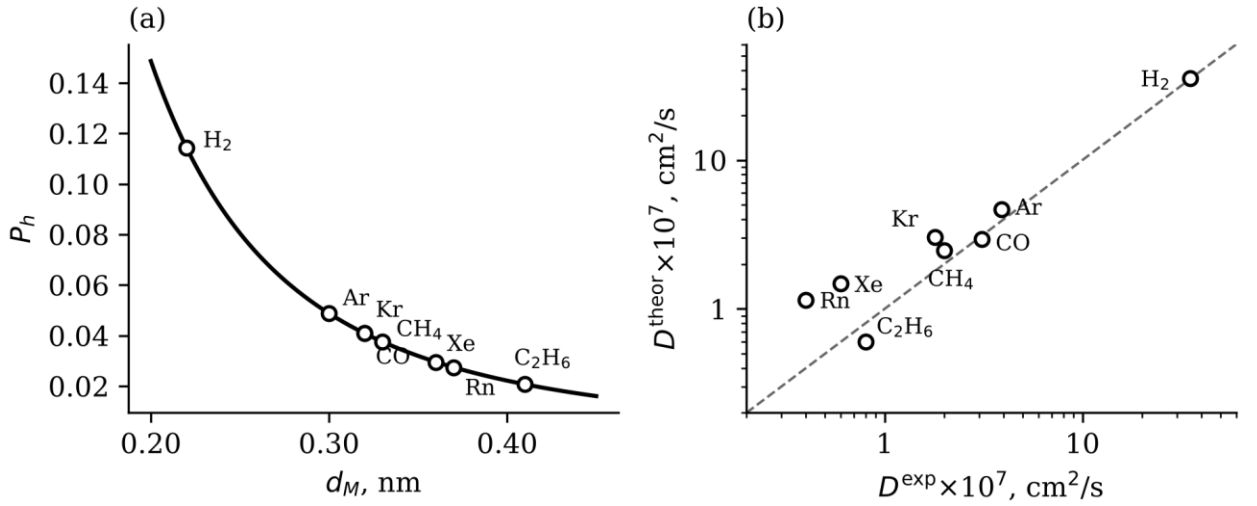



Figure 1 – Modelling results: (a) dependence of $P_h$ on $d_M$ (curve – Eq. (2), points – gases from Table 1); (b) comparison of $D^{theor}$ and $D^{exp}$ (dashed line – line of equality)

According to (3) and (4), the gas flux is proportional to $P_h(d_M)$, i.e. it is determined by the multifractal structure of the amorphous phase. $O_2$ molecules are close in size to argon atoms; therefore, the model predicts $P_h \approx 0.05$ for them, while methane ($P_h = 0.038$) characterizes biogas losses through polymer gas holders and pipelines. Thus, reducing the fraction of accessible free volume by controlling the crystallinity, orientation and heat treatment of PE is a direct way to decrease the oxygen permeability of silage films and grain bags. A similar approach is advisable for polymer seals of machine units operating in gas and air-oil media [10].

**Conclusions.** A multifractal model of gas diffusion in solid polyethylene has been substantiated, according to which the diffusion coefficient equals the product of the melt diffusion coefficient and the probability $P_h = (d_M/c)^{-2.75}$ of finding a free-volume microvoid accessible to a gas molecule. For $H_2$, CO, $CH_4$, $C_2H_6$ and Ar, the discrepancy between calculated and experimental values does not exceed 25 %, and the correlation coefficient of the logarithms is 0.94. The model has a simple physical meaning and makes it possible to predict the gas permeability of silage and greenhouse films, grain bags and polymer parts of AIC machinery from the parameters of the material nanostructure.

## References

1. Espí, E., Salmerón, A., Fontecha, A., García, Y., & Real, A. I. (2006). Plastic films for agricultural applications. *Journal of Plastic Film & Sheeting*, 22(2), 85–102.

2. Wilkinson, J. M., & Fenlon, J. S. (2014). A meta-analysis comparing standard polyethylene and oxygen barrier film in terms of losses during storage and aerobic stability of silage. *Grass and Forage Science*, 69(3), 385–392. https://doi.org/10.1111/gfs.12087
3. Orosz, S., Wilkinson, J. M., Wigley, S., Bíró, Z., & Galló, J. (2013). Microbial status, aerobic stability and fermentation of maize silage sealed with an oxygen barrier film or standard polyethylene film. *Agricultural and Food Science*, 22(1), 182–188. https://doi.org/10.23986/afsci.6705
4. Zubiekhina-Khaiiat, O., Hruban, V., Lymar, O., & Marchenko, D. (2026). Designing technologies for strengthening tractor and self-propelled machine parts in agricultural conditions. *Ukrainian Black Sea Region Agrarian Science*, 30(1), 46. https://doi.org/10.56407/bs.agrarian/1.2026.46
5. Lymar, O., & Marchenko, D. (2022). Prospects for the application of restoring electric arc coatings in the repair of machines and mechanisms. In *2022 IEEE 4th International Conference on Modern Electrical and Energy System (MEES)* (pp. 1–4). https://doi.org/10.1109/MEES58014.2022.10005709
6. Klopffer, M. H., & Flaconnèche, B. (2001). Transport properties of gases in polymers: Bibliographic review. *Oil & Gas Science and Technology*, 56(3), 223–244. https://doi.org/10.2516/ogst:2001021
7. Flaconnèche, B., Martin, J., & Klopffer, M. H. (2001). Permeability, diffusion and solubility of gases in polyethylene, polyamide 11 and poly(vinylidene fluoride). *Oil & Gas Science and Technology*, 56(3), 261–278. https://doi.org/10.2516/ogst:2001023
8. Michaels, A. S., & Bixler, H. J. (1961). Flow of gases through polyethylene. *Journal of Polymer Science*, 50, 413–439.
9. Lymar, O., & Khomenko, V. (2026). Enhancing the physical and mechanical properties of materials through annealing in the recovery range. In *Innovations in Agricultural Engineering: Proceedings of the International Scientific and Practical Conference* (Mykolaiv, April 7–9, 2026) (pp. 41–43). MNAU.
10. Marchenko, D., Matvyeyeva, K., Lymar, O., & Kurepin, V. (2025). Enhancing the reliability and wear resistance of high-speed cutting tools through the use of ionized air-oil lubrication media in machine part restoration. *Problems of Tribology*, 30(4/118), 72–78. https://doi.org/10.31891/2079-1372-2025-118-4-72-78.

UDC 621.785.5:631.3

# FORMATION OF A WEAR-RESISTANT STRUCTURE ON THE NITRIDED SURFACE OF AGRICULTURAL MACHINERY PARTS MADE OF 51CRV4 STEEL AFTER LASER TREATMENT

***Marchenko D.D.**, PhD (Engineering), Associate Professor*
***Lymar O.O.**, PhD (Physics and Mathematics), Associate Professor*
*Mykolaiv National Agrarian University, Mykolaiv, Ukraine*

**Problem statement.** The operating efficiency of the machine and tractor fleet of the agro-industrial complex (AIC) is largely determined by the durability of parts operating under conditions of abrasive wear, alternating loads and corrosive environments. Failures of wearing parts account for more than half of all failures of agricultural machines [1], and domestically produced working tools have a service life 1.2–2 times shorter than imported analogues [2]. The most critical are the parts of the cylinder-piston group of tractor and combine harvester diesel engines, for which the permissible wear of the working surfaces is tenths of a millimeters, as well as spring working tools of tillage machines (cultivator tines, harrow teeth) made of chromium-vanadium spring steels of the 51CrV4 type (EN 10089, 1.8159; equivalent to AISI/SAE 6150). Therefore, an urgent scientific and practical task is to develop combined surface hardening technologies that ensure the formation of wear-resistant structures without reducing the toughness of the part core [3].

**Analysis of recent research and publications.** The experience of European, Japanese and American manufacturers confirms that laser hardening and thermal spraying are effective methods for increasing the service life of engine parts [4]. Laser treatment provides heating of the metal at a rate of about $10^6$ K/s in a small heating zone, which results in high cooling rates. During laser exposure, the following stages are distinguished: absorption of the light flux and energy transfer to